Electrochromic Performance of Viologen-Modified Periodic Mesoporous Nanocrystalline Anatase Electrodes

ARTICLE *in* NANO LETTERS · JUNE 2004

Impact Factor: 13.59 · DOI: 10.1021/nl049484d

5 AUTHORS, INCLUDING:

Sung Yeun Choi
BASF SE
15 PUBLICATIONS **966** CITATIONS
SEE PROFILE

Marc Mamak
Procter & Gamble
28 PUBLICATIONS **1,351** CITATIONS
SEE PROFILE

Neil Coombs
University of Toronto
120 PUBLICATIONS **8,579** CITATIONS
SEE PROFILE

NANO LETTERS

2004
Vol. 4, No. 7
1231−1235

Electrochromic Performance of Viologen-Modified Periodic Mesoporous Nanocrystalline Anatase Electrodes

Sung Yeun Choi,[†] Marc Mamak,[†] Neil Coombs,[†] Naveen Chopra,[‡] and Geoffrey A. Ozin*,[†]

Materials Chemistry Research Group, Department of Chemistry, 80 St. George Street, University of Toronto, Toronto, Ontario, Canada M5S 3H6, and Xerox Research Centre of Canada, 2660 Speakman Drive, Mississauga, Ontario, Canada L5K 2L1

Received April 6, 2004; Revised Manuscript Received May 20, 2004

ABSTRACT

We report for the first time on the electrochromic performance of viologen-modified periodic mesoporous nanocrystalline anatase, denoted meso-nc-TiO_2-V(2+). Electrodes fashioned from meso-nc-TiO_2-V(2+) were found to display enhanced color contrast yet have similar conduction band edge energy level and electron percolation ability as electrodes made from viologen-modified nanocrystalline titania, nc-TiO_2-V(2+). This performance can be attributed to the uniform and ordered mesopore architecture, the nanocrystalline anatase wall structure, and the large accessible surface area for tethering viologen molecules.

With the explosive growth of broadband communications and wireless technologies, the demand for inexpensive thin film lightweight display devices with paper-like readability and ultralow power consumption has increased. One promising technology is the electrochromic (EC) device based upon dye-modified semiconductor electrodes. Such a device has advantages compared to intercalation EC electrodes, based on materials such as tungsten oxide, due to much improved time response and enhanced color contrast especially for display technologies such as electronic paper or billboards.[1−3] The heart of the device is a working electrode composed of a nanocrystalline semiconductor, usually an n-type metal oxide, which has been modified with an electrochromophoric molecular species, most often a redox active viologen derivative, chemically tethered to the surface of the nanocrystalline electrode. The efficiency of this system is based upon fast interfacial electron transfer between the nanocrystalline electrode and the anchored chromophore along with optical amplification brought about by the large surface area of the nanocrystals, which enables high chromophore loading per unit area of the electrode.[1d]

Nanocrystalline titania (nc-TiO_2) has been successfully used for this purpose, resulting in a high efficiency electrochromic device mainly due to the intrinsic properties of the nanocrystalline titania electrode, such as transparency to visible light, electronic conductivity, high surface affinity toward certain ligands, and large surface area.[1−4] In this context, mesoporous titania (meso-TiO_2) is of considerable interest because of its high surface area and uniform and well-ordered mesopores, which should facilitate the entry of dye molecules into pores and anchoring of them to anatase nanocrystals that comprise the channel walls.[5] There are many reports for the synthesis and photocatalytic/photoelectrochemical properties of meso-TiO_2,[6,7] however, no reports yet exist concerning its electrochromic (EC) behavior.

In this communication, we report for the first time on the EC performance of a new generation of viologen-modified periodic mesoporous nanocrystalline titania, meso-nc-TiO_2-V(2+), thin film electrodes, particularly concerning color contrast and color switching speed, electrochemical redox potentials and reversibility, transient absorption change during cycling, and color cycling stability. The uniquely robust channel walls of meso-nc-TiO_2 support a relatively large average anatase crystallite size, which favorably impacts electrochromic reversibility and overall cell performance. The following abbreviations will be used throughout the text to clearly distinguish the three types of titania that we are concerned with, namely: nc-TiO_2, conventional nanocrystalline anatase titania; meso-TiO_2, periodic mesoporous titania calcined at 350 °C; meso-nc-TiO_2, periodic mesoporous titania calcined at 400 °C. Viologen-modified analogues of these materials are denoted as nc-TiO_2-V(2+), meso-TiO_2-V(2+), and meso-nc-TiO_2-V(2+), respectively.

Meso-nc-TiO_2 thin film electrodes were prepared using procedures described in a recent report.[8] Meso-nc-TiO_2 synthesized by this method utilizes 1-butanol as solvent and has a 2-D structure with hexagonally close-packed mesopores

* Corresponding author E-mail: gozin@chem.utoronto.ca.
[†] University of Toronto.
[‡] XRCC.

10.1021/nl049484d CCC: $27.50
Published on Web 06/17/2004

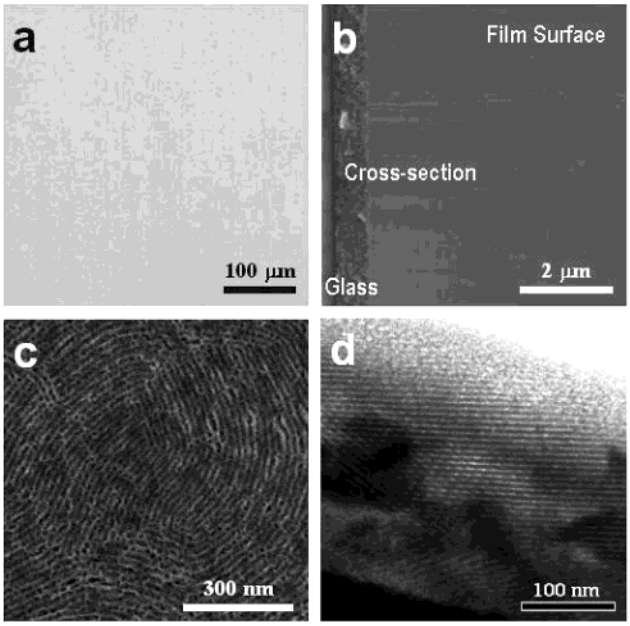

Figure 1. Optical microscope image (a), SEM images (Hitachi S-5200 SEM) (b, c), and TEM image (FEI Technai 20) (d) for crack-free meso-nc-TiO_2 film after calcination at 400 °C for 4 h. Top views (a, c), and cross-sectional views (b, d).

and channel walls made of 8∼10 nm anatase nanocrystallites depending on the calcination temperature.

Thin film electrodes of meso-nc-TiO_2 were prepared by spin coating (2400 rpm, 20 s) fresh reactant solution, molar composition $1Ti(EtO)_4/2HCl/0.013$ P123/9 1-butanol, onto a transparent conductive oxide (TCO) substrate (ITO, Evaporated Coatings Inc, ECI949, < 25 ohms/sq, or SnO_2:F coated glass, Pilkington, TEC8, < 9 ohms/sq) and aged in a humidity chamber for 2 days at 20 °C/80% relative humidity (RH). As-synthesized films were subsequently calcined at 350 °C and 400 °C for 4 h in air. As mentioned earlier, from this point forward, to distinguish the periodic mesoporous titania thin films calcined at 350 °C and 400 °C, they will be denoted as meso-TiO_2 and meso-nc-TiO_2, respectively. The obtained optically transparent meso-nc-TiO_2 films were observed to display a crack-free surface down to the scale of the mesostructure and over the entire film area (1.5 × 1.5 cm^2) even after calcination at 400 °C as shown in optical microscope and HRSEM images (Figure 1a, b, and c) with a well-defined 2-D hexagonal mesostructure as seen in the cross-section TEM image (Figure 1d). The average thickness of calcined films was estimated from TEM and SEM to be ca. 500 nm. The size of anatase nanocrystallites comprising the channel walls from HRTEM was ca. 6−10 nm.

To compare the electrochromic performance of meso-TiO_2 and meso-nc-TiO_2 thin film electrodes with nc-TiO_2, viologen dye (bis-(2-phosphonoethyl)-4,4′-bipyridinum dichloride) and nc-TiO_2 thin film electrodes were prepared by previously reported methods.[2]

Electrochemical investigations (Solartron 1287 potentiostat/galvanostat) were performed on thin film TiO_2 electrodes modified with the viologen from an aqueous solution (0.02 M) over 24 h.[2] For the cyclic voltammetry, a 3-electrode cell was prepared with the viologen-modified TiO_2 thin film (ca. 1 × 1 cm^2) as a working electrode, platinum gauze as a counter electrode, and Ag/AgCl sat. KCl (aq) as a reference electrode. A sandwich cell for spectroscopic investigation was constructed from a working electrode of viologen-modified TiO_2 (TiO_2−V(2+), 1.5 × 1.5 cm^2) on a TCO substrate and a counter electrode of bare TCO,[1b,f,3] and sealed using a thermoplastic sealant (Surlyn 1702, DuPont). All electrochemical measurements were conducted in acetonitrile/0.5 M $LiClO_4$ deaerated by bubbling with dry N_2 for 20 min prior to experiments.

Figure 2a shows a comparison of the cyclic voltammograms (CVs) obtained for 20 mV/s scan speed for meso-nc-TiO_2-V(2+) and nc-TiO_2 electrodes. Both electrodes color blue during the reduction scan between −0.55 and −0.75 V due to the single reduced viologen cation radical species. At potentials more negative than −0.75 V, the electrodes turned pale yellow due to the doubly reduced viologen, and when the potential decreased below −0.9 V, the TiO_2-V(2+) electrodes turned dark blue due to insertion of Li^+ cations into open sites within the anatase lattice. During the oxidation scan, reverse coloration from dark blue to pale yellow to blue and finally back to the original transparent state was observed in both cases. The obtained $E_{1/2}$ values of the first and the second redox peaks of viologen are −0.57 V and −0.93 V vs Ag/AgCl sat. KCl (aq) reference electrode, respectively. These redox potentials and CV peak shapes are similar to those previously reported.[1,2] In the case of meso-TiO_2, the redox properties of the tethered viologen were found to be quite different (Figure 2b). During the first reduction scan, the meso-TiO_2-V(2+) electrode behaved similarly to the meso-nc-TiO_2-V(2+) and nc-TiO_2-V(2+) electrodes, except the relatively narrow first reduction peak appeared at the slightly lower potential of −0.7 V. However, in the first oxidation scan, the color change of the meso-TiO_2-V(2+) electrode ceased at the blue state, never to return to the original transparent state. After the first cycle, the color of this electrode now changed between blue (V+•), pale yellow (V), and dark blue (Li^+ intercalated state), whereas the first redox pair corresponding to the V(+•) blue state and the V(2+) transparent state completely disappeared from the CV scan.

To summarize our observations up to this point, the meso-TiO_2-V(2+) electrode exhibited an irreversible first redox reaction of viologen, whereas the meso-nc-TiO_2-V(2+) electrode behaved similarly to the nc-TiO_2-V(2+) electrode and showed reversible viologen redox electrochemistry.

Upon closer inspection, however, the CVs obtained at 5 mV/s scan speed (designed to reduce capacitance effects, Figure 2c) reveal a notable difference between meso-nc-TiO_2 and nc-TiO_2 electrodes with respect to peak shape and redox peak potentials. In the case of the meso-nc-TiO_2-V(2+) electrode, an asymmetric first redox peak pair is apparent, whereas the nc-TiO_2-V(2+) electrode shows a relatively symmetric redox peak pair. Furthermore, the meso-nc-TiO_2-V(2+) electrode shows a narrower reduction peak at −0.62 V than the corresponding reduction peak for the nc-TiO_2-V(2+) electrode, although both occur at the same potential. Conversely, the meso-nc-TiO_2-V(2+) electrode exhibits a

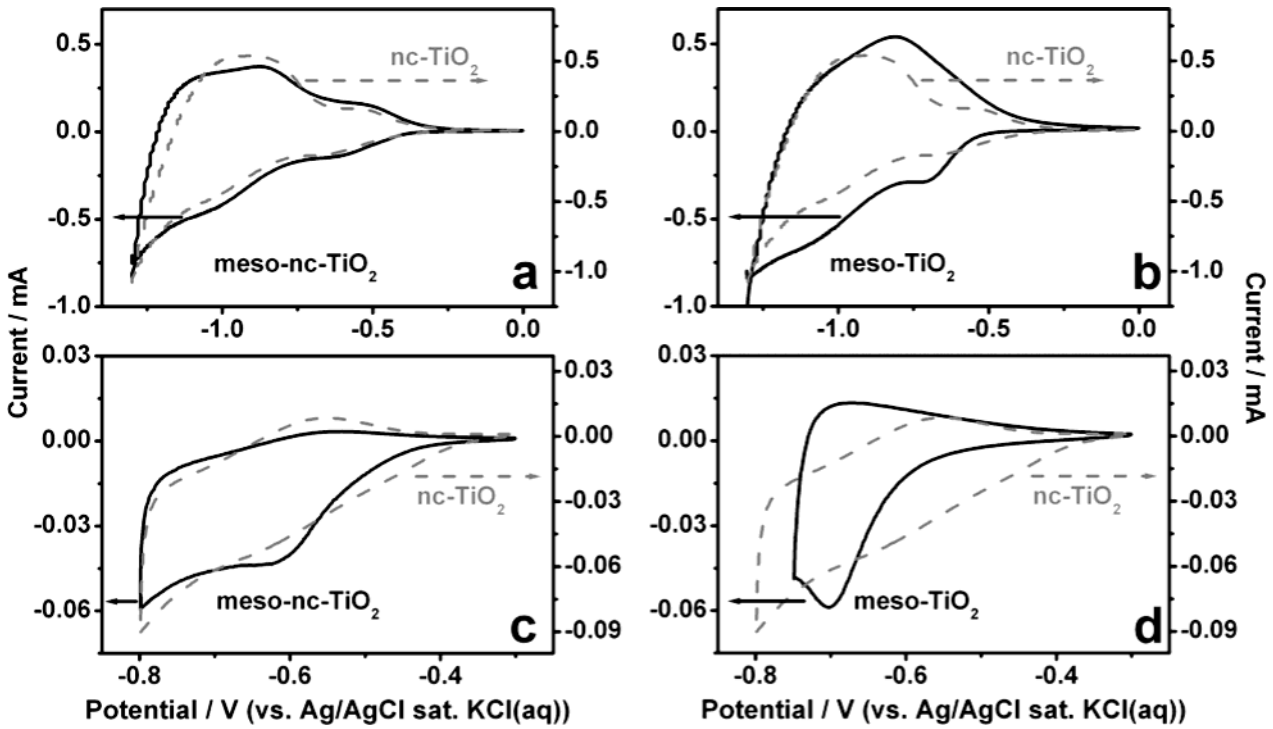

Figure 2. Cyclic voltammograms of bis-(2-phosphonoethyl)-4,4′-bipyridinum dichloride anchored on meso-nc-TiO_2 (a and c, black solid line, left scale), meso-TiO_2 (b and d, black solid line, left scale), and nc-TiO_2 (gray dashed line, right scale) thin film electrodes in 0.5 M $LiClO_4$ acetonitrile electrolyte. (a, b) scan range $-1.3 \sim 0$ V, scan rate 20 mV/s. (c, d) scan range $-0.8 \sim -0.3$ V, scan rate 5 mV/s.

much broader oxidation peak at − 0.53 V, which is shifted approximately 300 mV positive compared to nc-TiO_2-V(2+). This implies that the reduction process for the tethered viologen is more facile than the oxidation of the viologen cation radical on the meso-nc-TiO_2-V(2+) electrode. In the case of the meso-TiO_2-V(2+) electrode at the same scan speed, a much narrower reduction peak of tethered viologen appears in the first reduction scan, after which no further redox events were observed upon reaching the blue state (Figure 2d).

These results can be rationalized by taking into account the well-known relationship between the conduction band edge (CBE) of the titania electrode and first redox potential of the viologen, while keeping in mind the influence of the quantum size effect of nanocrystalline anatase upon the position of the CBE (Scheme 1). According to previous reports[1d,e] the reversible operation of this system demands that the position of the CBE of the titania electrode lie below the first redox potential of the chosen viologen. If the CBE of the TiO_2 electrode is located higher than the first redox potential of the chosen viologen, charge trapping will occur on the viologen species, leading to an irreversible first redox process. It has been reported that the channel walls of meso-TiO_2 are comprised of nanocrystalline anatase of much smaller dimensions (∼8.8 nm for meso-TiO_2 and ∼10.3 nm for meso-nc-TiO_2)[8] than in nanocrystalline titania devices (10−25 nm).[4,9] As a result, the CBE of meso-TiO_2 with nanocrystalline channel walls is expected to be driven higher than nc-TiO_2 due to the quantum size effect.[10] Depending on the size of the nanocrystallites, the position of the CBE may be either driven sufficiently high to cause an irreversible redox process, illustrated in Scheme 1, resulting in charge trapping on the tethered viologen species, such as we observe for the meso-TiO_2 electrode, or it may be just high enough to affect only the speed of the redox process, such as observed for the meso-nc-TiO_2 electrode. Our CV results imply that the energy level of the CBE of the meso-nc-TiO_2 electrode is similar to that of nc-TiO_2, therefore reversible coloration/bleaching of the EC cell is facilitated. In contradistinction, the meso-TiO_2 electrode suffers from an irreversible redox process, which is manifest as semi-permanent coloration of the device. The key distinguishing feature responsible for the difference in reversibility between meso-TiO_2 and meso-nc-TiO_2 electrodes appears to originate from the divisions of the nanocrystals comprising the channel walls.

Scheme 1. Representation of the Influence of the Conduction Band Edge on the Reversibility of Tethered Viologen Species on nc-TiO_2, meso-nc-TiO_2, and meso-TiO_2 Electrodes

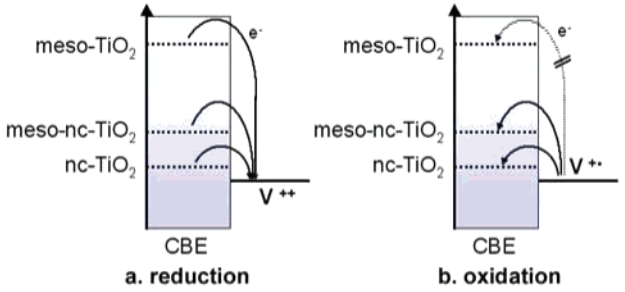

To compare the color contrast, color switching time, and transient absorption change during cycling of the meso-nc-TiO_2-V(2+) electrode with the nc-TiO_2-V(2+) electrode, a

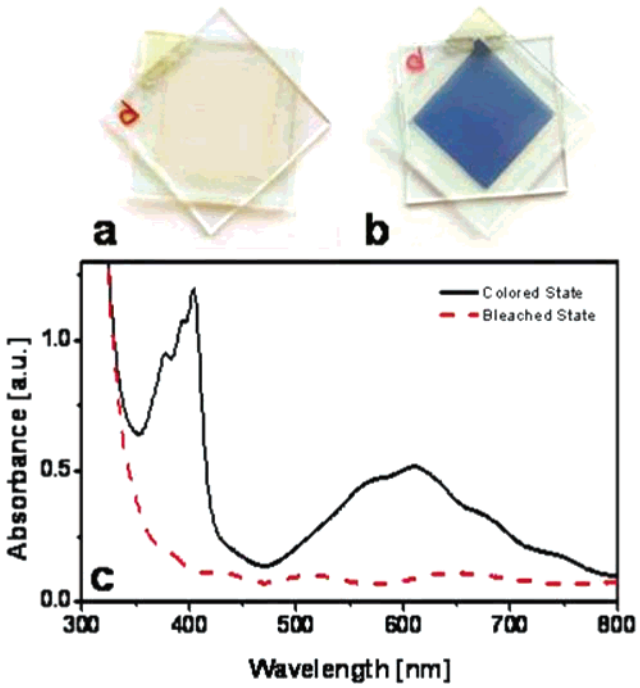

Figure 3. Photographic images of the thin film meso-nc-TiO_2-V(2+) electrochromic cell before (a) and after (b) applying −2.5 V, and UV−vis absorption spectra (c) of the same samples before (dashed line) and after (solid line) applying −2.5 V.

spectroscopic investigation of the electrochromic behavior was carried out using a sandwich cell. Prior to the application of an external voltage, the assembled sandwich cell was entirely transparent, as shown in Figure 3a. In the corresponding UV−vis absorption spectrum (dashed line in Figure 3c), no absorption peaks were observed between 400 and 800 nm. When the meso-nc-TiO_2-V(2+) electrode is negatively biased by an external voltage of 2.5 V versus the bare TCO counter electrode, the transparent EC cell rapidly changed to deep blue as observed in Figure 3b. The spectrum of the blue electrode is shown as a solid line in Figure 3c and is diagnostic of the spectrum of the cation radical state of the tethered viologen, namely meso-nc-TiO_2-V(+•). The absorbance difference at 608 nm between the bleached and colored state of meso-nc-TiO_2 EC cell is about 0.43. This observation is promising when compared to a similarly assembled EC cell with a nc-TiO_2-V(2+) electrode that is 12 times greater in thickness (6 μm) and has an absorbance difference of ca. 0.6.

The EC absorbance change, ΔA, of a thin film TiO_2 electrode can be expressed according to eq 1:[1e,f]

$$\Delta A = \Gamma_R \epsilon_R 1000 \qquad (1)$$

where Γ_R is the apparent surface concentration of viologen on the electrode and ϵ_R is the extinction coefficient of the viologen radical in solution. The coefficient 1000 is a dimension correction factor and the ϵ_R of the viologen cation radical can be taken as 14000 $M^{-1}cm^{-1}$ at 608 nm.[2] We have calculated the apparent surface concentration of viologen on the thin film meso-nc-TiO_2-V(2+) electrode to be 3.1×10^{-8} mol/cm^2 based on the obtained ΔA, whereas on the nc-TiO_2-V(2+) electrode it is 4.3×10^{-8} mol/cm^2. Taking into consideration the difference in thickness between the nc-TiO_2 film (6 μm) versus the meso-nc-TiO_2 film (ca. 500 nm), a thickness normalized apparent surface concentration value of the meso-nc-TiO_2 EC electrode is calculated as 8.6 times greater than the nc-TiO_2-V(2+) EC electrode. Moreover, this is 3.6 times higher than the best ever reported value for a nc-TiO_2 EC cell,[1e] which showed a ΔA of 1.2 for a 5 μm thick nc-TiO_2 film electrode.

The enhanced color contrast of meso-nc-TiO_2 is likely related to the amplification brought about by the well-ordered mesopores, uniform mesopore size and shape, and high surface area of meso-nc-TiO_2, which together enable a greater volume density of tethered viologens. Though the reported specific surface area measured through N_2 sorption of nc-TiO_2 can be as large as 145 m^2/g,[9] which is roughly 84% of the surface area of meso-nc-TiO_2 synthesized by the 1-butanol method (172 m^2/g for a bulk gel[8]), the practical accessible surface area of nc-TiO_2 to relatively large molecules such as viologens is expected to be low due to the irregular pore structure and shape defined by a random network of disordered and agglomerated nanocrystallites.

The color switching speed of the meso-nc-TiO_2-V(2+) and nc-TiO_2-V(2+) EC cells were measured following the application of 2.5 V versus a bare TCO electrode for 60 s, where both TiO_2-V(2+) electrodes were biased negative for coloration and positive for bleaching (Figure 4a). The obtained coloration and bleaching times, defined as the time taken for the absorbance to change by two-thirds the difference between the steady-state absorbance in the bleached and colored states,[2] of the meso-nc-TiO_2-V(2+) EC cell are 2.1 and 0.9 s, respectively. For direct comparison, an identically fabricated device based on an nc-TiO_2-V(2+) EC cell shows 7.0 s for coloration and 0.2 s for bleaching. These color switching speeds correlate well with the CV data presented in Figure 2c, where the meso-nc-TiO_2-V(2+) electrode shows a faster coloration speed but slower bleaching speed than the nc-TiO_2-V(2+) electrode.

The long-term stability of the meso-nc-TiO_2 EC cell was tested under ambient conditions by subjecting it to 100 electrochromic cycles. Each electrochromic cycle consisted of applying a potential of 2.5 V versus a bare TCO electrode for 10 s, which biased the viologen-modified meso-nc-TiO_2 electrode negative for coloration and positive for bleaching. As shown in Figure 4b, the meso-nc-TiO_2 EC cell was completely bleached at the end of every cycle; however, the color contrast gradually declined with increasing cycles, finally settling to around 51% of the absorbance of the first cycle at the 100th cycle. As seen in Figure 4b, the color contrast of a similarly constructed and electrochemically tested nc-TiO_2-V(2+) EC cell also gradually decreased over the same number of cycles and with comparable rates to meso-nc-TiO_2-V(2+) EC cell. Complete bleaching of the meso-nc-TiO_2 EC cell after each cycle is actually noteworthy since, as mentioned earlier, the meso-TiO_2 electrode suffers from an irreversible redox process, which leads to incomplete bleaching and semi-permanent blue coloration of the device

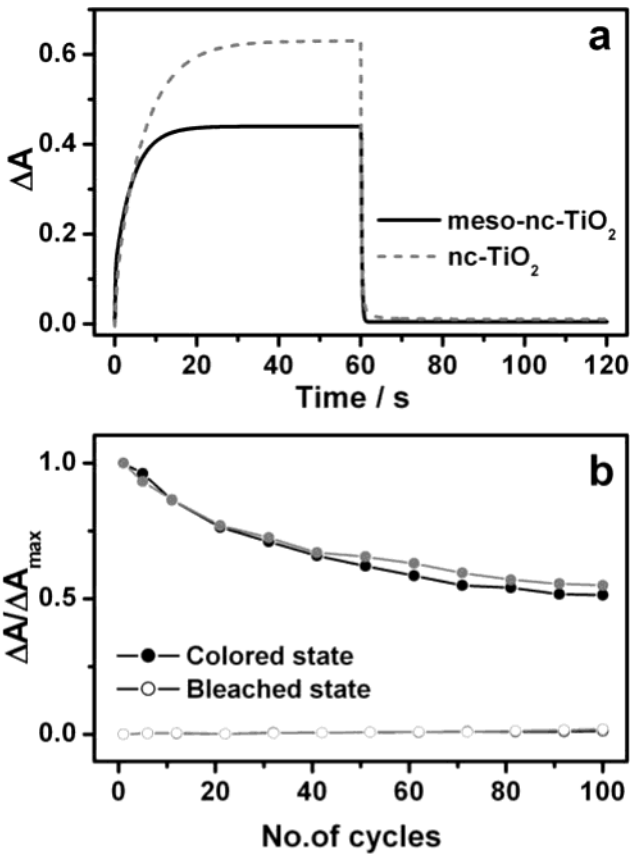

Figure 4. (a) Transient absorbance at 608 nm of the electrochromic cell made of viologen-modified meso-nc-TiO_2 (solid line) and nc-TiO_2 (dashed line) electrodes following application of −2.5 V and 2.5 V, which voltage biases the viologen-modified TiO_2 electrode with respect to the bare TCO electrode. (b) Relative absorbance profile of the colored state (filled circles) and bleached state (open circles) at 608 nm of the electrochromic cell made of meso-nc-TiO_2 (black line) and nc-TiO_2 (gray line) during electrochromic cycling (100 cycles, 1 cycle: −2.5 V, 10 s/2.5 V, 10 s) as a function of the number of cycles.

due to the adversely shifted CBE position. The results in Figure 4 hold much promise for the use of meso-nc-TiO_2-based electrodes in engineered electrochromic devices.

In conclusion, we have investigated the electrochromic performance of a new generation of periodic mesoporous thin film electrodes denoted as meso-nc-TiO_2-V(2+). This study shows the well-ordered mesostructured, nanocrystalline titania electrode to exhibit similar color switching speed and reversibility as nanocrystalline titania but with better performance in terms of color contrast. This performance can be attributed to meso-nc-TiO_2 being composed of a contiguous pathway of well-connected anatase nanocrystallites arranged into a well-defined mesoporous architecture, which results in a greater volume density of tethered chromophore molecules. Further investigation of the electrical properties of our meso-nc-TiO_2-V(2+) electrodes are in progress, as are studies aimed at the optimization of electrochemical cell conditions to improve the coloration speed, coloration efficiency, mechanical durability, and long-term stability, especially under ambient conditions.

Acknowledgment. G.A.O. is Government of Canada Research Chair in Materials Chemistry. The authors thank the Xerox Research Centre of Canada, NSERC, and the University of Toronto for sustained financial support. Valuable discussions with Dr. Sebastian Polarz are greatly appreciated. SEM imaging was performed at the CFI funded Centre of Nanostructure Imaging at the Chemistry Department, University of Toronto.

References

(1) (a) Cinnsealach, R.; Boschloo, G.; Nagaraja Rao, S.; Fitzmaurice, D. *Sol. Energy Mater. Sol. Cells* **1998**, *55*, 215. (b) Cinnsealach, R.; Boschloo, G.; Nagaraja Rao, S.; Fitzmaurice, D. *Sol. Energy Mater. Sol. Cells* **1999**, *57*, 107. (c) Bonhôte, P.; Gogniat, E.; Grätzel, M.; Ashrit, P. V. *Thin Solid Films* **1999**, *350*, 269. (d) Bonhôte, P.; Gogniat, E.; Campus, F.; Walder, L.; Grätzel, M. *Displays* **1999**, *20*, 137. (e) Campus, F.; Bonhôte, P.; Grätzel, M.; Heinen, S.; Walder, L. *Sol. Energy Mater. Sol. Cells* **1999**, *56*, 281. (f) Felderhoff, M.; Heinen, S.; Molisho, N.; Webersinn, S.; Walder, L. *Helv. Chim. Acta* **2000**, *83*, 181.

(2) Cummins, D.; Boschloo, G.; Ryan, M.; Corr, D.; Nagaraja Rao, S.; Fitzmaurice, D. *Phys. Chem. B* **2000**, *104*, 11449.

(3) Bach, U.; Corr, D.; Lupo, D.; Pichot, F.; Ryan, M. *Adv. Mater.* **2002**, *14*, 845.

(4) (a) Hagfeldt, A.; Grätzel, M. *Chem. Rev.* **1995**, *95*, 49. (b) Gerfin, T.; Grätzel, M.; Walder, L. *Prog. Inorg. Chem.* **1997**, *44*, 345.

(5) (a) Antonelli, D. M.; Ying, J. Y. *Angew. Chem., Int. Ed. Engl.* **1995**, *34*, 2014. (b) Yang, P.; Zhao, D.; Margolese, D. I.; Chmelka, B. F.; Stucky, G. D. *Nature* **1998**, *396*, 152. (c) Grosso, D.; Soler-Illia, G. J. A. A.; Babonneau, F.; Sanchez, C.; Albouy, P. A.; Brunet-Bruneau, A.; Balkenende, A. R. *Adv. Mater.* **2001**, *13*, 1085. (d) Yun, H.-S.; Miyazawa, K.; Zhou, H.; Honma, I.; Kuwabara, M. *Adv. Mater.* **2001**, *13*, 1377. (e) Schüth, F. *Chem. Mater.* **2001**, *13*, 3184. (f) Soler-Illia, G. J. A. A.; Sanchez, C.; Lebeau, B.; Patarin, J. *Chem. Rev.* **2002**, *102*, 4093.

(6) (a) Honma, I.; Zhou, H. S.; Kundu, D.; Endo, A. *Adv. Mater.* **2000**, *12*, 1529. (b) Klotz, M.; Ayral, A.; Guizard, C.; Cot, L. *J. Mater. Chem.* **2000**, *10*, 663. (c) Soler-Illia, G. J. A. A.; Scolan, E.; Louis, A.; Albouy, P. A.; Sanchez, C. *New J. Chem.* **2001**, *25*, 156. (d) Hwang, Y. K.; Lee, K. C.; Kwon, Y. U. *Chem. Commun.* **2001**, *18*, 1738. (e) Alberius, P. C. A.; Frindell, K. L.; Hayward, R. C.; Kramer, E. J.; Stucky, G. D.; Chmelka, B. F. *Chem. Mater.* **2002**, *14*, 3284. (f) Crepaldi, E. L.; Soler-Illia, G. J. A. A.; Grosso, D.; Sanchez, C. *New J. Chem.* **2003**, *27*, 9.

(7) (a) Baeck, S.; Choi, K.; Jaramillo, T. F.; Stucky, G. D. *Adv. Mater.* **2003**, *15*, 1269. (b) Cakley, K. M.; Liu, Y.; McGehee, M. D.; Frindell, K. L.; Stucky, G. D. *Adv. Funct. Mater.* **2003**, *13*, 301. (c) Shchukin, D. G.; Caruso, R. A. *Adv. Funct. Mater.* **2003**, *13*, 789.

(8) Choi, S. Y.; Mamak, M.; Coombs, N.; Chopra, N.; Ozin, G. A. *Adv. Funct. Mater.* **2004**, *14*, 335.

(9) Barbe, C. J.; Arendse, F.; Comte, P.; Jirousek, M.; Lenzmann, F.; Shklover, V.; Grätzel, M. *J. Am. Ceram. Soc.* **1997**, *80*, 3157.

(10) Reddy, K. M.; Reddy, C. V. G.; Manorama, S. V. *J. Solid State Chem.* **2001**, *158*, 180.

NL049484D